

Multiphoton Absorption and Emission by Interaction of Swift Electrons with Evanescent Light Fields

F. Javier García de Abajo,^{*,†} Ana Asenjo-García,[†] and Mathieu Kociak[‡]

[†]Instituto de Óptica—CSIC, Serrano 121, 28006 Madrid, Spain, and [‡]Laboratoire de Physique des Solides, CNRS, UMR8502, Université Paris Sud XI, F 91405 Orsay, France

ABSTRACT We introduce a theory to describe the interaction of swift electrons with strong evanescent light fields. This allows us to explain recent experimental results of multiple energy losses and gains for electrons passing near illuminated nanostructures. A complex evolution of the electron state over attosecond time scales is unveiled, giving rise to non-Poissonian distributions of multiphoton features in the electron spectra. Prospects for application to nanoscale-resolved transmission electron microscopy and spectroscopy are discussed.

KEYWORDS Electron energy gain, attosecond electron dynamics, electron microscopy, EELS, electron–light interaction

Transmission electron microscopes are ubiquitous in nanoscience because they can yield images with subangstrom space resolution.¹ Simultaneous analysis of electron energy losses can add information on the optical response with nanometer detail.² Unfortunately, the best reported energy resolution (~ 0.1 eV) is still insufficient to resolve fine spectral features commonly encountered in nanostructures. It has been suggested^{3,4} that electrons picking up photon-generated energy losses or gains from externally supplied light can largely improve energy resolution down to the light spectral width. An experimental advance in this direction has been recently made by Barwick et al.,⁵ who demonstrated multiphoton absorption by pulsed electrons passing near nanostructures in coincidence with pulsed laser irradiation. These authors managed to image carbon nanotubes and silver nanowires by resorting to energy-filtered accelerated electrons. They also reported time-resolved measurements as a function of the delay between the photon and electron pulses with subpicosecond resolution, whose duration (>200 fs) was unfortunately too large to resolve the dynamics of electronic collective modes in these nanostructures (lifetime \sim tens of femtoseconds).

Except for high-order processes requiring intense illumination (for example, in the Kapitza–Dirac effect⁶), the electron–photon coupling is weak in free space due to energy-momentum mismatch. However, a sampled nanostructure can break the mismatch by supplying extra momentum through induced light fields, as observed in illuminated gratings (inverse Smith–Purcell effect⁷). Likewise, thermal phonons were long realized to produce electron energy gains,⁸ and so were plasmons generated by other

electrons in an intense beam.⁹ The interaction of swift electrons and evanescent light fields can therefore be a practical way of sampling fine spectral features in nanostructures, excited under finely tuned external illumination.

In this Letter, we present a theory of multiple energy losses and gains of electrons traversing a light field induced near a nanostructure. The light and the electrons are realistically described as classical and quantum-mechanical pulses, respectively. The results are compared with available experiments for electrons interacting with silver nanowires.⁵ Although the interaction time lies in the subfemtosecond domain, the electron wave function is found to exhibit a complex evolution that gives rise to oscillations in probability when varying the laser intensity or when considering different numbers of exchanged photons. Besides their intrinsic interest, we study these phenomena for their relevance in on-going efforts aimed at developing space-resolved energy-gain spectroscopy.⁴

We focus on the system described in Figure 1a, in which an energetic electron pulse passes near a nanostructure in coincidence with a light pulse. The light–electron interaction is mainly driven by the evanescent optical field. Current ultrafast-optics technology allows subpicosecond pulses to be produced with light peak intensities of several GW/cm^2 , leading to multiphoton absorption and emission as shown for example in the spectra of Figure 1b. The spectral features display a marked non-Poissonian distribution that suggests an important role of coherence between subsequent single-photon events.

The parameters used in Figure 1 are taken to reproduce Barwick et al.’s experiment:⁵ the photon pulse has a duration of 220 fs; the light focus is so large that it can be approximated by a plane wave at the position of the sample; the pulse of 200 keV electrons has a fitted duration of 424

* Corresponding author, jga@cfmac.csic.es.

Received for review: 02/20/2010

Published on Web: 04/23/2010

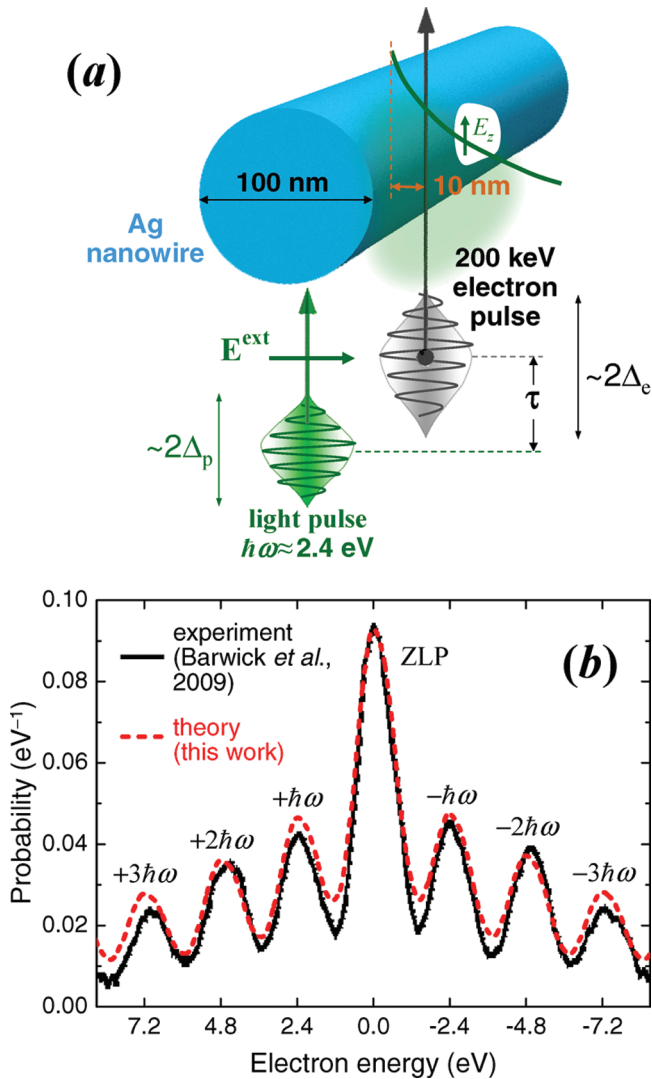


FIGURE 1. (a) Sketch of the system under consideration. An electron pulse passes near a nanostructure in coincidence with a light pulse. The electron–photon interaction is mediated by evanescent components of the induced light field (see exponentially decaying light field intensity to the right of the nanostructure and the E_z electric field component along the electron trajectory). Parameters used throughout this work are shown by text insets. (b) Transmitted electron spectrum revealing multiphoton absorption and emission events under the conditions of (a). The photon pulse has central energy $\hbar\omega = 2.4$ eV and duration of 220 fs. The electron pulse is centered around 200 keV. Solid curve: experimental data from ref 5. Broken curve: present theory, convoluted with experimental zero-loss peak (ZLP) and calculated for a peak light intensity of 3 GW/cm², an electron pulse duration of 424 fs and delay $\tau = 0$.

fs, in good agreement with the experimental estimate;⁵ the sample consists of a long 100 nm thick silver nanowire; both electron and photon pulses propagate along nearly the same direction, perpendicular to the wire; finally, no exact values are reported on the exact light intensity and range of impact parameters used in the experiment, so we have chosen the electron to pass at a distance of 10 nm from the silver surface, rather than integrating over electron impact parameters, and we use a light intensity of 3 GW/cm². We model the experiment by solving the quantum-mechanical evolu-

tion of the electron in its interaction with the evanescent light field; the latter is obtained by solving Maxwell's equations for the silver wire using the boundary element method,¹⁰ using the tabulated frequency-dependent dielectric function of silver to represent the response of the metal.¹¹

It should be mentioned that the experimental results so far available⁵ tell us nothing new about the nanostructures under consideration, although they provide compelling evidence of a complex subfemtosecond electron evolution, as we discuss below. The technique should be capable of yielding details on the optical response of nanostructures in the time domain, with a temporal resolution dictated by the duration of the electron and photon pulses. The latter should be still greatly reduced in order to study short-lived excitations such as plasmons. As it stands, the technique is however unique in its potential to image evanescent light fields with nanometer resolution (e.g., the standing waves of an interference optical corral).

Electron-Light Interaction. Low-energy exchanges between swift electrons and a specimen can be safely described by only considering electron motion along the beam direction \hat{z} .¹⁰ For instance, since the electron momentum (≈ 250 Å⁻¹ at 200 keV kinetic energy) is large compared to the wave function spreading along transversal directions ($\lesssim 0.1$ Å⁻¹ for a typical beam diameter $\gtrsim 1$ Å), we are allowed to approximate the electron–light interaction as $\propto \mathbf{E} \cdot \nabla \psi \approx E_z \partial \psi / \partial z$. The resulting coupling Hamiltonian reduces to

$$H_l(z, t) = \frac{-e\hbar}{m_e \omega} [E_z(z, t) - E_z^*(z, t)] \frac{\partial}{\partial z} \quad (1)$$

where ω is the central light frequency and

$$E_z(z, t) = \mathcal{E}_z(z) \exp[-i\omega t - (t + \tau)^2 / \Delta_p^2] \quad (2)$$

is the component of the total electric field parallel to the beam. This light field incorporates a Gaussian profile of temporal duration $\sim 2\Delta_p$ (95% of the light intensity lies in the time interval $|t + \tau| < \Delta_p$) and delay $-\tau$ relative to the electron pulse (see below). We consider the pulse to have a narrow spectral width $\Delta\omega \sim \Delta_p^{-1} \ll \omega$, over which the dispersion in the response of the sample can be overlooked. Incidentally, our using a classical light field in H_l is justified when the light pulse contains a large number of photons.

Incident Electron Wave Function. We write the wave function of the unperturbed incident electron as $\psi_0(z, t) = \psi_{k_0}^G(z, t)$, where

$$\psi_{k_0}^G(z, t) = \mathbf{N}_k \exp[ikz - i\epsilon_k t - (t - z/v_k)^2 / \Delta_e^2] \quad (3)$$

is a Gaussian electron pulse of temporal duration $\sim 2\Delta_e$, the normalization constant $|\mathbf{N}_k|^2 = ((\pi/2)^{1/2} \Delta_e v_k)^{-1}$ is introduced

to have one electron per pulse, $\hbar\varepsilon_k = c(\hbar^2k^2 + m_e^2c^2)^{1/2}$ is the electron energy, and $v_k = \partial\varepsilon_k/\partial k$ is the pulse group velocity ($v_k \approx \hbar k/m_e$ at low kinetic energies). We assume small spreading in electron energy and momentum around $\hbar\varepsilon_{k_0}$ and $\hbar k_0$, respectively, or equivalently, $\varepsilon_{k_0}\Delta_e \gg 1$.

Full Electron Wave Function. Using the Lippmann–Schwinger equation, the total electron wave function is

$$\psi(z, t) = \psi_0(z, t) + \int dz' dt' G(z - z', t - t') H_l(z', t') \psi(z', t') \quad (4)$$

where

$$\begin{aligned} G(z - z', t - t') &= \frac{1}{4\pi^2\hbar} \int d\varepsilon_k \int dq \frac{\exp[iq(z - z') - i\varepsilon_k(t - t')]}{\varepsilon_k - \varepsilon_q + i0^+} \\ &\approx \frac{-i}{2\pi\hbar} \int dk \exp[ik|z - z'| - i\varepsilon_k(t - t')] \quad (5) \end{aligned}$$

is the Green function for motion along z . We have approximated the pole $\varepsilon_k - \varepsilon_q \approx (k - q)v_k$ to derive the last expression and extend the integral to negative k , since the main contribution to eq 4 is strongly peaked around $k \approx k_0$.

We solve eq 4 using the perturbation expansion

$$\psi(z, t) = \sum_{N=0}^{\infty} (GH_l)^N \psi_0 \equiv \sum_{N=0}^{\infty} \psi_N(z, t) \quad (6)$$

where the sum is extended over scattering orders N . Each new order of scattering raises by one the number of exchanged virtual photons, which involves either absorption (term proportional to \mathcal{E}_z in H_l) or emission (term in \mathcal{E}_z^*). Consecutive virtual emissions and absorptions can take place, so that the N th term in eq 6 includes electrons that have gained or lost L real photons, under the condition $|L| \leq N$. Therefore, it is reasonable to expand ψ_N in terms of Gaussian waves $\psi_{k_L}^G$ as

$$\psi_N(z, t) = \sum_{L=-N}^N \psi_{k_L}^G(z, t) F_L^N(z) e^{-N(t-z/v_{k_L}+t')^2/\Delta_p^2} \quad (7)$$

where k_L is the electron wave vector after exchanging L real photons (i.e., it corresponds to electrons of energy $\hbar\varepsilon_0 + \hbar\omega$), and the exponential factor accounts for the reduction in laser-pulse N -order intensity at the time of interaction. In the nonrecoil approximation,¹⁰ one has $k_L = k_0 + L\omega/v$, where v is the electron central velocity ($v \approx 0.7c$ at 200 keV).

We expect F_L^N to be time-independent and vary smoothly with z . A proof of this intuition can be found by induction, using the explicit expressions of eqs 1–7 to write

$$\begin{aligned} \psi_{N+1}(z, t) &= GH_l \psi_N = \\ &= \frac{ie}{m_e\omega} \sum_{L=-N}^N \mathbf{k}_{k_L} \int dz' \int dt' [\mathcal{E}_z(z') I_+ - \mathcal{E}_z^*(z') I_-] \times \\ &\quad \left(ik_L + \frac{\partial}{\partial z'} \right) F_L^N(z') e^{-(t'-z'/v_{k_L})^2/\Delta_p^2} e^{-N(t'-z'/v_{k_L}+t')^2/\Delta_p^2} e^{-(t'+t')^2/\Delta_p^2} \quad (8) \end{aligned}$$

where

$$I_{\pm} = \int \frac{dk}{2\pi} e^{ik|z-z'|} e^{ik_L z'} e^{-i\varepsilon_k(t-t')} e^{-i\varepsilon_{k_L} t'} e^{\mp i\omega t'}$$

At this point, it should be noted that the wavelength of a 200 keV electron is only $2\pi/k_0 \approx 2.5$ pm, so that for $z < z'$, the functions I_{\pm} oscillate fast with z' compared to the remaining factors in the integrand of eq 8 (for example, light fields should be nearly constant over distances of several nanometers). Therefore, only for $z > z'$ is I_{\pm} going to contribute non-negligibly to eq 8, because then the oscillations of wave vectors k and k_L are partially compensated. We find

$$I_{\pm} \approx \exp[i(k_{L\pm 1}z - \varepsilon_{k_{L\pm 1}}t \mp i\omega z'/v)] \theta(z - z') \times \delta[z - z' - v_{k_{L\pm 1}}(t - t')]$$

Now, the δ function allows us to directly carry out the t' integral of eq 8 and to write ψ_{N+1} as in eq 7, with $N \rightarrow N + 1$. The resulting functions F_L^{N+1} are subject to the recursion relation

$$\begin{aligned} F_L^{N+1}(z) &= \frac{e}{m_e v \omega} \int_{-\infty}^z dz' \left[\mathcal{E}_z(z') e^{-i\omega z'/v} \left(i \frac{\partial}{\partial z'} - k_L \right) F_{L-1}^N(z') - \right. \\ &\quad \left. \mathcal{E}_z^*(z') e^{i\omega z'/v} \left(i \frac{\partial}{\partial z'} - k_L \right) F_{L+1}^N(z') \right] \quad (9) \end{aligned}$$

where the starting value is $F_0^0 = 1$ and we define $F_L^N = 0$ for $|L| > N$. In the derivation of eq 9 we have assumed that the light Gaussian profile does not vary significantly over a distance equal to the interaction path length Δz (i.e., $\Delta_p c \gg \Delta z$). Interestingly, this recursion produces $F_L^N = 0$ unless $N + L$ is an even number, so that it mixes contributions of orders $N = |L|, |L| + 2, |L| + 4, \dots$, within each final k_L .

Transmitted Spectrum. The transmitted electron spectrum exhibits peaks centered around energies $\hbar\varepsilon_{k_L}$, equally spaced by $\hbar\omega$. The width of each peak is of the order of $\hbar(\Delta_e^{-1} + L\Delta_p^{-1}) \ll \hbar\omega$, and therefore, different Gaussian-wave components $\psi_{k_L}^G$ in eq 7 contribute to separate peaks

L with negligible overlap. We can calculate the probability that the electron ends up having momentum around a given k_L from the contribution to the time-integral of the electron current ($\text{Im}\{\psi^* \partial\psi/\partial z\}$) produced by terms of fixed L in eqs 6 and 7. It is convenient to do this outside the interaction region, where ε_z is negligible and the functions $F_L^N(z)$ converge to constant values C_L^N . One obtains

$$P_L = \sum_{N=|L|}^{\infty} \sum_{N'=|L|}^{\infty} C_L^N (C_L^{N'})^* \frac{\exp\left\{-\frac{(N+N')(\tau/\Delta_p)^2}{1 + [(N+N')/2](\Delta_e/\Delta_p)^2}\right\}}{\sqrt{1 + \frac{N+N'}{2}(\Delta_e/\Delta_p)^2}} \quad (10)$$

Interestingly, the probabilities depend on the pulse durations and delay only through the ratios τ/Δ_p and Δ_e/Δ_p .

We solve the recursion relation (9) by iteration and achieve numerical convergence in $\sum_L P_L = 1$ with an error $<10^{-3}$. The electric field \mathcal{E}_z is obtained from the boundary element method.¹⁰ Figure 1b shows a characteristic result compared to measured data for electrons passing near a silver nanowire.⁵ Experimental parameters have been implemented in the theory, and although no values were reported for the electron–wire distance and the Δ_e/Δ_p ratio, we find that they are not critical for the comparison (see caption of Figure 1). In particular, the electron pulse should have a duration of the order of a second light pulse used in the photoemission effect from which the electron is produced. Furthermore, the electron–wire distance should be assimilable to an effective light strength. Figure 1b demonstrates that the present theory is capable of explaining the observed non-Poissonian multiphoton distribution.

Point-Electron and Continuous-Wave Limits. An interesting result is obtained in the $\Delta_p \gg \Delta_e$ limit of eq 10 (i.e., when the electron pulse lasts much less than the photon pulse)

$$P_L = \left| \sum_{N=|L|}^{\infty} C_L^N \exp[-N(\tau/\Delta_p)^2] \right|^2 \quad (11)$$

where the exponential factor reflects the attenuation of the photon pulse with τ (eq 2), as observed by the electron during interaction (i.e., at times $|t|/\Delta_p \ll 1$). Equation 11 can also be derived from the stationary perturbation theory, describing the electron as a sum of plane waves along z . Incidentally, the probability derived in ref 4 corresponds to the low light-intensity limit of eq 11 ($N = 1$ term).

We show in Figure 2 a characteristic example of the evolution of multiphoton probabilities with the intensity of the external light. At low intensities, the elastic signal is slowly depopulated and single-photon peaks show up on

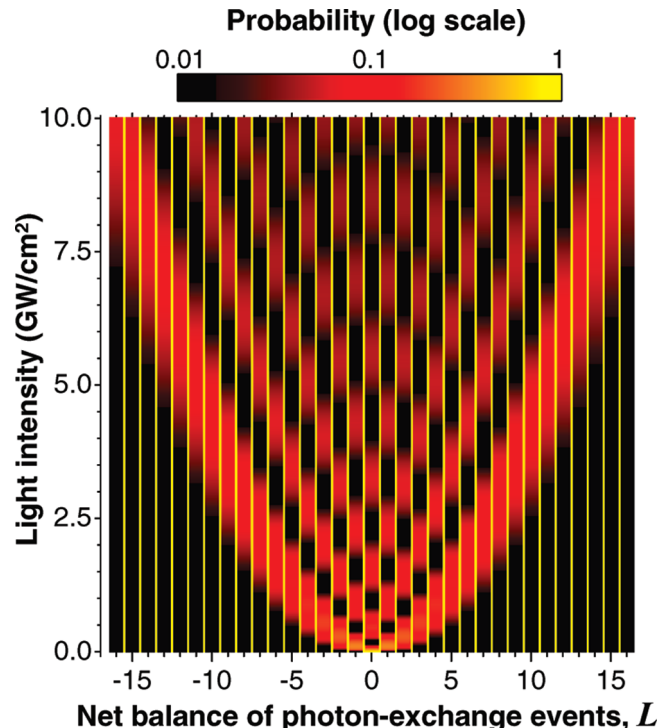


FIGURE 2. Probability of multiphoton emission ($L > 0$) and absorption ($L < 0$) under the conditions of Figure 1a for $\Delta_p \gg \Delta_e$. The probabilities P_L (eq 11) are represented as a function of light intensity for different net numbers of exchanged photons L .

either side of it. As the intensity increases, multiphoton processes take over, and simultaneously, some of the lowest-order peaks become depopulated. The effect of multiple photon absorptions and emissions is to produce oscillations in electron probability with the net number of exchanged photons. These oscillations are the result of interference between different multiple-order processes (i.e., different N values) contributing the same final electron state L . Coherence becomes critical, and a dramatic departure from Poissonian statistics is observed.

Effect of Pulse Durations and Delay. The oscillations of P_L with L are washed out when Δ_e/Δ_p increases, as shown in Figure 3a. The amplitude cancelations observed by interference of subsequent N contributions in Figure 2 are simply smeared out when virtual photon exchanges can take place over an increasing period of time $\sim \Delta_e$ (Figure 3a). In particular, these oscillations are already gone under the experimental conditions of ref 5. Nevertheless, there is physical room for exploring the lowest region of Figure 3a ($\Delta_e \ll \Delta_p$) because the electron period is many orders of magnitude shorter than the light period.

The effect of pulse delay simply consists in reducing the effective interaction strength, thus producing a decrease in multiphoton probabilities with increasing τ (Figure 3b).

Time evolution. Figure 4 shows the evolution of the electron wave function with time over the interaction region. It clearly reveals the transfer of electron probability from $L = 0$ to $L = \pm 1$ at $t \approx -0.3$ fs, and the subsequent transfer

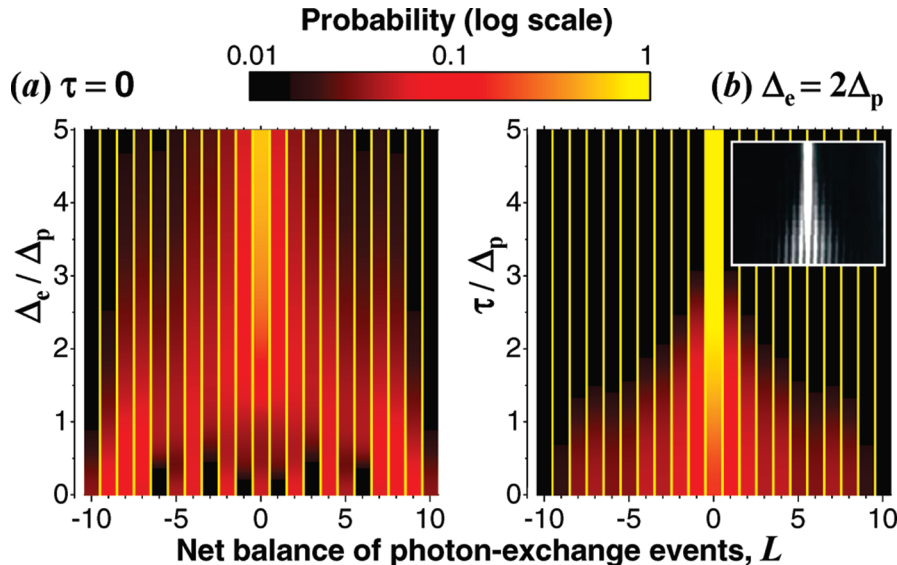


FIGURE 3. Influence of electron pulse duration Δ_e and pulse delay τ in multiphoton probabilities under the conditions of Figure 1a. (a) Dependence of P_L (eq 10) on Δ_e/Δ_p for $\tau = 0$. (b) Dependence of P_L on τ/Δ_p for $\Delta_e = 2\Delta_p$. The peak light intensity is 3 GW/cm^2 . The inset of (b) shows measurements from ref 5 for a carbon nanotube over a similar range of τ/Δ_p .

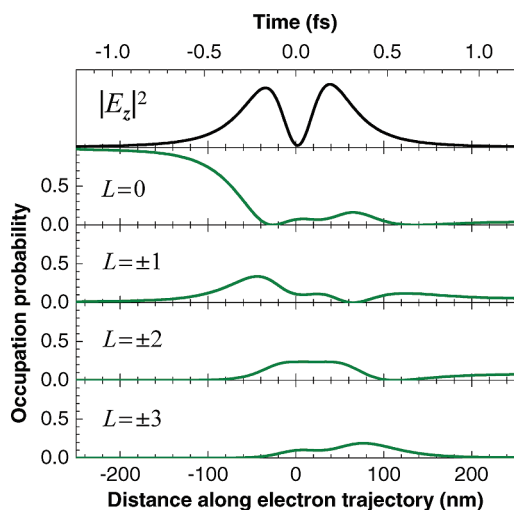


FIGURE 4. Evolution of the electron wave function over the interaction region under the conditions of Figure 1a for $\Delta_p \gg \Delta_e$ and $\tau = 0$. We represent the intensity of the electric-field component along the electron trajectory $|E_z(z)|^2$ (see Figure 1a) and the occupation probability of electron states after a net exchange of L photons $(|\sum_N F_L^N(z)|^2)$ for the lowest values of L . The peak light intensity is 1 GW/cm^2 .

from $L = \pm 1$ back to $L = 0$ and also to $L = \pm 2$ around $t \approx 0$. These results further corroborate our interpretation of multiple virtual photon exchanges leading to interference effects in the final distribution of electron states.

In conclusion, the interaction of swift electrons with intense induced light fields in nanostructures gives rise to a complex evolution of the electron states over characteristic subfemtosecond interaction times. This results in non-Poissonian distributions of energy gains and losses in the

transmitted electron spectra. Although we have considered the light to be spectrally narrow, an extension of our theory would permit speculating with applications to time-resolved spectroscopy, involving the frequency dependence of the sample response when using spectrally broader light. Alternatively, time- and space-resolved spectroscopy could be performed by varying the central light frequency ω , with energy and time resolution limited by the uncertainty principle. Finally, access to nonlinear spectroscopy could be granted by finer analysis of spectral features under intense illumination.

Acknowledgment. F.J.G.A. wants to thank Archie Howie for useful discussions. This work has been supported by the Spanish MICINN (MAT2007-66050 and Consolider NanoLight.es).

REFERENCES AND NOTES

- (1) Nellist, P. D.; Chisholm, M. F.; Dellby, N.; Krivanek, O. L.; Murfitt, M. F.; Szilagyi, Z. S.; Lupini, A. R.; Borisevich, A.; Sides, W. H., Jr.; Pennycook, S. J. *Science* **2004**, *305*, 1741.
- (2) Egerton, R. F. *Ultramicroscopy* **2007**, *107*, 575–586.
- (3) Howie, A. *Inst. Phys. Conf. Ser.* **1999**, *161*, 311–314.
- (4) Garcia de Abajo, F. J.; Kociak, M. *New J. Phys.* **2008**, *10*, No. 073035.
- (5) Barwick, B.; Flannigan, D. J.; Zewail, A. H. *Nature* **2009**, *462*, 902–906.
- (6) Batelaan, H. *Rev. Mod. Phys.* **2007**, *79*, 929–941.
- (7) Mizuno, K.; Pae, J.; Nozokido, T.; Furuya, K. *Nature* **1987**, *328*, 45–47.
- (8) Boersch, H.; Geiger, J.; Stickel, W. *Phys. Rev. Lett.* **1966**, *17*, 379–381.
- (9) Schilling, J.; Raether, H. *J. Phys.: Condens. Matter* **1973**, *6*, L358–L360.
- (10) Garcia de Abajo, F. J. *Rev. Mod. Phys.* **2010**, *82*, 209–275.
- (11) Johnson, P. B.; Christy, R. W. *Phys. Rev. B* **1972**, *6*, 4370–4379.